

# Thickness dependence of the stability of the charge-ordered state in $\text{Pr}_{0.5}\text{Ca}_{0.5}\text{MnO}_3$ thin films.

W. Prellier, Ch. Simon, A.M. Haghiri-Gosnet, B. Mercey and B. Raveau  
*Laboratoire CRISMAT, CNRS UMR 6508, ISMRA et Université de Caen, Bd du  
Maréchal Juin, 14050 Caen Cedex, FRANCE.*

(October 28, 2018)

## Abstract

Thin films of the charge-ordered (CO) compound  $\text{Pr}_{0.5}\text{Ca}_{0.5}\text{MnO}_3$  have been deposited onto (100)-oriented  $\text{SrTiO}_3$  substrates using the Pulsed Laser Deposition technique. Magnetization and transport properties are measured when the thickness of the film is varied. While the thinner films do not exhibit any temperature induced insulator-metal transition under an applied magnetic field up to 9T, for thickness larger than  $1100\text{\AA}$  a 5T magnetic field is sufficient to melt the CO state. For this latest film, we have measured the temperature-field phase diagram. Compared to the bulk material, it indicates that the robustness of the CO state in thin films is strongly depending on the strains and the thickness. We proposed an explanation based on the distortion of the cell of the film.

Recently, perovskite type manganites such as  $\text{RE}_{1-x}\text{A}_x\text{MnO}_3$  (RE and A are respectively a rare-earth and an alkaline-earth ion), have renewed interest due to their properties of colossal magnetoresistance (CMR), a huge decrease in resistance when applying a magnetic field<sup>1-5</sup>. Since most of the technological applications require thin films, it is essential to understand the effects of the substrate-induced strains on the properties of these manganites. These materials are very sensitive to the strains and even very small perturbations may result in observable effects on the properties. These effects have indeed been studied experimentally on various compounds<sup>6-10</sup>. Moreover, among all the properties of these manganite materials, the phenomenon of charge-ordering (CO) is probably one of the most remarkable effects. It appears for certain value of x and particular average A-site cation radi ( $\langle r_A \rangle$ ). It corresponds to an ordering of the charges in two different Mn sublattices. In fact, the metallic state becomes unstable, below a certain temperature ( $T_{CO}$ ) and the material goes to an insulating state.  $T_{CO}$  decreases with increasing field and the insulating CO state can be totally suppressed by the application of an external magnetic field<sup>10-12</sup>. As an example, a 25T magnetic field is required to melt the CO state in the bulk  $\text{Pr}_{0.5}\text{Ca}_{0.5}\text{MnO}_3$ <sup>14</sup>.

But, we have shown recently that, when this compound is synthesized as a thin film on  $\text{SrTiO}_3$  (i.e. with a tensile stress), the melting magnetic field is reduced to 6T<sup>15</sup>, whereas a value of 9T is not sufficient when the film is grown on  $\text{LaAlO}_3$  to collapse this metastable state<sup>16</sup>. This means that uniaxial strain ( $\sim 1-2\%$  in the plane) leads to dramatic changes as compared to the bulk material. Following the same idea, one would expect that the relaxation of the strains along the direction normal to the plane of the substrate (i.e when the thickness of the film is varying) should also induce changes in the electronic properties. For these reasons, it is also interesting to vary the thickness of the films grown on  $\text{SrTiO}_3$ .

In the present work, we have studied the effects of the thickness and the strains upon the structural and physical properties of  $\text{Pr}_{0.5}\text{Ca}_{0.5}\text{MnO}_3$  (PCMO) thin films grown on  $\text{SrTiO}_3$  using the Pulsed Laser Deposition technique. We have particularly considered the changes in lattice parameters, transport measurements and magnetization. On the basis of these results, we have determined a temperature-field phase diagram for CO thin films and compared it

to the bulk material.

Thin films of PCMO were grown in-situ using the Pulsed Laser Deposition (PLD) technique on [100]-SrTiO<sub>3</sub> substrates (cubic with  $a=3.905\text{\AA}$ ). Detailed optimization of the growth procedure was completed and described previously<sup>15,16</sup>. The structural study was carried out by X-Ray diffraction (XRD) using a Seifert XRD 3000P for the  $\theta-2\theta$  scans and a Philips MRD X'pert for the in-plane measurements (Cu K $\alpha$ ,  $\lambda=1.5406\text{\AA}$ ). The in-plane parameters were obtained from the  $(103)_C$  reflection (where  $c$  refers to the ideal cubic perovskite cell). Direct current (dc) resistivity ( $\rho$ ) was measured by a four-probe method with a Quantum Design PPMS and magnetization ( $M$ ) was recorded using a Quantum Design MPMS SQUID magnetometer as a function of the temperature ( $T$ ) and the magnetic field ( $H$ ). The composition of the films was checked by energy-dispersive scattering analyses. It is homogenous and corresponds exactly to the composition of the target (i.e. Pr<sub>0.5</sub>Ca<sub>0.5</sub>Mn) in the limit of the accuracy.

The structure of bulk Pr<sub>0.5</sub>Ca<sub>0.5</sub>MnO<sub>3</sub> is orthorhombic ( $Pnma$ ) with  $a=5.395\text{\AA}$ ,  $b=7.612\text{\AA}$  and  $c=5.403\text{\AA}$ <sup>17</sup>. Fig. 1 shows a typical  $\theta-2\theta$  scan recorded for a film of (750 $\text{\AA}$ ). Note that the same pattern is obtained for all of the films. As already reported, the film is a single phase, [010]-oriented, i.e. with the [010] axis perpendicular to the substrate plane<sup>15</sup>. This surprising orientation results from the lattice mismatch. Indeed, the mismatch ( $s$ ) between the film and the substrate can be evaluated using the formula  $\sigma = 100 * (\sigma_S - \sigma_F) / \sigma_S$  (where  $a_S$  and  $a_F$  respectively refer to the lattice parameter of the substrate and the film). The smaller mismatch on LaAlO<sub>3</sub> is obtained for a [010]-axis in the plane ( $\sigma_{LAO} = -0.4\%$ ), i.e. [101]-axis perpendicular to the substrate plane. In contrast, the smaller mismatch on SrTiO<sub>3</sub> ( $\sigma_{STO} = 2.2\%$ ) is found for a [101]-axis in the plane and thus a [010]-axis normal to the surface of the substrate as found experimentally<sup>15</sup>. The sharp peaks at 90° intervals in the  $\phi$ -scan of the PCMO film (see inset of Fig.1) make evident the existence of a complete in-plane texture of the film. From the XRD, the out-of-plane parameter of this 750 $\text{\AA}$  film is calculated to be 3.79 $\text{\AA}$ . However, as a consequence of the biaxial strains, the lattice parameter is slightly different when the thickness of the film is changing. Similar results

are obtained for the in-plane lattice parameter and the corresponding data are plotted in Fig.2. When the film is very thin (150Å), the in-plane parameter is nearly equal to the one of the substrate (3.88Å vs 3.9Å for STO). When the thickness of the film is increasing, the in-plane parameter is decreasing whereas in the mean time, the out-of-plane parameter is increasing. For large thickness (>1200Å), both lattice parameters tend towards a value close to the bulk. However, they never reach exactly the bulk values and the film is never fully relaxed. Note that the cell volume is preserved constant and equal to that of the bulk ( $\sim 56\text{\AA}^3$  referring to the perovskite cell). Moreover, the temperature dependence of these cell parameters should be very different from that of bulk samples. It was shown previously that the orthorhombic distortion induced by the CO ordering is strongly reduced by the presence of the substrate, preventing the locking of the  $q$  value of the CO on the  $\frac{1}{2}$  value contrary to the bulk sample of the same composition, leading to  $q=0.45$  for the thicker film<sup>15</sup>.

Fig.3 shows the temperature dependence with different applied magnetic fields (0, 5T and 9T) for three films thickness. In the absence of applied field, one always observes a semiconducting behavior with an anomaly around 225K corresponding to the charge-ordered transition (this value is close to the one found in the bulk material<sup>14</sup>). On the contrary, the results are drastically different under application of external magnetic fields. Application of a magnetic field up to our maximum value (9T) has almost no effect on the thinner film (150Å): the film is still semiconducting and the magnetoresistance is very small (Fig.3a). For the intermediate thickness (750Å), while a 5T magnetic field keeps the film semiconducting, a 9T renders it metallic with a  $T_{MI}$  close to 125K (see Fig.3b). This feature is a typical characteristic of the melting of the CO state. On the thicker film (1100Å), the melting magnetic field is reducing to 5T (Fig.3c). The thickness dependence of the properties suggests that the strains play an important role in determining the melting magnetic field. When the thickness of the film is increasing, there is a reduction of the strain on the film at room temperature. However, the properties of the film do not approach those of the bulk as the substrate-induced strain reduces. In PCMO single crystal, with a 6T magnetic field, the material remains insulating, whereas the 1100Å film becomes metallic<sup>18</sup>.

The magnetic field dependence of the resistivity at various temperatures is shown in Fig. 4. The resistivity shows an important decrease on a logarithmic scale at a critical field ( $H_C$ ) indicating the field-induced melting of the CO state. This field-induced insulator to metal transition, which accompanies the collapsing of the CO state takes place below  $T_{CO}$ . The critical fields in the field-increasing scan and in the field decreasing scan will respectively be represented by  $H_c^+$  and  $H_c^-$ . This decrease can be viewed as CMR of about five orders of magnitude at 75K. A clear hysteresis (between the lower and the upper critical fields) is seen at these temperatures as previously reported on several CO compounds<sup>12,18</sup>. This hysteretic region is more pronounced when the temperature is decreasing. The temperature dependence of the large hysteresis region is a feature of a first order transition and has been extensively studied for the composition  $\text{Nd}_{0.5}\text{Sr}_{0.5}\text{MnO}_3$  in ref.<sup>12</sup>. Similar results can be observed in magnetization measurements (fig. 5), though our maximum field is then 5T. From the resistivity measurements, we can deduce a phase diagram for the 1100Å film (Fig. 6). Two remarks should be pointed out. First, as already mentioned, the transition of the metastable state (i.e. a field-induced metallic state) is easier or requires a lower field in case of a 1100Å thin film than in the bulk<sup>18</sup>. Second, the shape of the  $H - T$  phase diagram is totally different as compared to the bulk single crystal  $\text{Pr}_{0.5}\text{Ca}_{0.5}\text{MnO}_3$ . In fact, this phase diagram of the 1100Å film has almost the same profile as  $\text{Pr}_{1-x}\text{Ca}_x\text{MnO}_3$  single crystal with  $0.35 < x < 0.45$ . The hysteretic region grows when the temperature is decreasing and rapidly vanishes under 8T. This can be explained by the variation of the q vector. Indeed, the value of the q vector of the CO modulation (0.45) is also similar to that of  $\text{Pr}_{1-x}\text{Ca}_x\text{MnO}_3$  single crystal with  $0.35 < x < 0.45$ , suggesting that the whole electronic structure is similar, though the charge transfer is different ( $x=0.5$  instead of 0.4 in  $\text{Pr}_{1-x}\text{Ca}_x\text{MnO}_3$ ). This was discussed in more detail in a previous paper<sup>16</sup>. In spite of this, the important new result is the thickness dependence of the film properties. The distortion induced by the CO cannot fully develop due to the strains imposed by the substrate. Consequently, the CO is limited to an incommensurate value leading to a less stable CO state, more sensitive to the magnetic field. In fact, a large CO gap in the density of states at the Fermi level is associated with a

very stable CO state<sup>19</sup>. As the thickness is decreasing, the in-plane cell parameter is going closer to the substrate value and it can be supposed that it also follows its temperature dependence leading to a large cell distortion. Thus, the substrate-induced strain can be measured by the lattice-distortion  $D$  of the film cell defined as the ratio between the in-plane and the out-of-plane parameters. The evolution of  $D$  vs thickness is plotted in the inset of Fig.2. As the lattice-distortion or equivalently the tolerance factor<sup>20</sup> is approaching one, the distortion of the perovskite cell is decreasing. In the mean time, the critical field required to melt the CO state is also decreasing. This behavior is similar to that observed for bulk materials  $\text{RE}_{1-x}\text{Ca}_x\text{MnO}_3$ , whose CO state is destabilized when the tolerance factor is getting close to one (or the size of the A-site cation is increasing)<sup>13,21</sup>. In return, the present evolution of the magnetotransport properties cannot be directly compared to that of the bulk compound  $\text{Pr}_{0.5}\text{Ca}_{0.5}\text{MnO}_3$ , due to the different nature of the cell distortion imposed by the substrate.

In summary, we have shown that the melting magnetic field of the insulating charge-ordered state, in  $\text{Pr}_{0.5}\text{Ca}_{0.5}\text{MnO}_3$  films, is strongly sensitive to the thickness of the film. While, the application of a magnetic field up to 9T has almost no effect on the resistivity on a very thin film, a 5T magnetic field can completely melt the CO state of a 1100Å thick film. The reduction of this critical magnetic field with the thickness can be explained by the distortion of the cell of the thin film. Finally, it appears, that an increase of the thickness in thin films under tensile strain has the same effect as decreasing the size of the A-site cation in bulk material: the stability of the CO state is decreasing in  $\text{Ln}_{0.5}\text{Ca}_{0.5}\text{MnO}_3$  when Ln goes from Y to La<sup>22</sup>.

The authors thank Dr. A. Maignan and Dr. R. Mahendiran for fruitful discussions.

## REFERENCES

- <sup>1</sup> R. Von Helmolt, J. Wecker, R. Holzapfel, L. Schultz, K. Samwer, Phys. Rev. Lett. 71, 2331 (1993).
- <sup>2</sup> K. Chahara, T. Ohno, M. Kasai Y. Kosono, App. Phys. Lett. 63, 1990 (1993).
- <sup>3</sup> M. McCormack, S. Jin, T. Tiefel, R.M. Fleming, J.M. Philips, R. Ramesh, App. Phys. Lett. 64, 3045 (1994).
- <sup>4</sup> T. Venkatesan, M. Rajeswari, Z-W. Dong, S.B. Ogale and R. Ramesh, Phil. Trans. R. Soc. London, 356, 1661 (1998).
- <sup>5</sup> S. Jin, T.H. Tiefel, M. McCormack, R.A. Fastnacht, R. Ramesh and L.H. Chen, Science 75, 3336 (1996).
- <sup>6</sup> A. Biswas, M. Rajeswari, R.C. Srivastava, Y.H. Li, T. Venkatesan, R.L. Greene and A.J. Millis, Phys. Rev. B 61, 9665 (2000).
- <sup>7</sup> W. Prellier, A. Biswas, M. Rajeswari, T. Venkatesan and R.L. Greene, App. Phys. Lett. 75, 397 (1999).
- <sup>8</sup> H.S. Wang, Q. Li, K. Kiu and C.L. Chien, App. Phys. Lett. 74, 2212 (1999).
- <sup>9</sup> J. O'Donnell, M. Onellion, M.S. Rzechowski, J.N. Eckstein and I. Bozovic, Phys. Rev. B 54, 6841 (1996).
- <sup>10</sup> J.Z. Sun, D.W. Abraham, R.A. Rao and C.B. Eom, App. Phys. Lett. 73, 3294 (1999).
- <sup>11</sup> E.O. Wollan and W.C. Koehler, Phys. Rev. 100, 545 (1950). Z. Jirak, S. Krupicka, Z. Sinsa, M. Dlouha and S. Vratislav, J. Magn. Magn. Mater. 53, 153 (1985).
- <sup>12</sup> H. Kuwahara, Y. Tomioka, A. Asamitsu, Y. Moritomo and Y. Tokura, Science 270, 961 (1995).
- <sup>13</sup> C.N.R. Rao, A. Arulraj, A.K. Cheetham and B. Raveau, J. Phys.: Condens. Matter. 12,

- R83 (2000).
- <sup>14</sup> M. Tokunaga, N. Miura, Y. Tomioka and Y. Tokura, Phys. Rev. B 57, 5259 (1998).
- <sup>15</sup> W. Prellier, A.M. Haghiri-Gosnet, B. Mercey, Ph. Lecoeur, M. Hervieu, Ch. Simon and B. Raveau, App. Phys. Lett. (2000) accepted.
- <sup>16</sup> A.M. Haghiri-Gosnet, M. Hervieu, Ch. Simon, B. Mercey and B. Raveau, J. App. Phys. (2000) to be published.
- <sup>17</sup> Z. Jirak, S. Krupicka, Z. Simsa, M. Doulka and S. Vratislma, J. Magn. Magn. Mat. 53, 153 (1985).
- <sup>18</sup> Y. Tomioka, A. Asamitsu, H. Kuwahara, Y. Moritomo and Y. Tokura, Phys. Rev. B 53, R1689 (1996).
- <sup>19</sup> A. Biswas, A.K. Raychaudhuri, R. Mahendiran, R. Mahesh and C.N.R Rao, J. Phys.: Condens. Matter. 9, L335 (1997).
- <sup>20</sup> V.R. Goldschmidt, Skr. Nor. Vidensk-Acad. Oslo, 1 Mat. Naturv. K1, 8 (1926).
- <sup>21</sup> A. Arulraj, P.N. Santhosh, R.S. Gopalan, A. Guha, A.K. Raychaudhuri, N. Kumar and C.N. R. Rao, J. Phys.: Condens. Matter. 10, 8497 (1998).
- <sup>22</sup> M. Respaud, A. Llobet, C. Frontera, C. Ritter, J.M. Broto, H. Rakoto, M. Goiran, J.L. Garcia-Munoz, Phys. Rev. B 61, 9014 (2000).

## I.



## FIGURE CAPTIONS

Fig.1 : Room temperature  $\theta - 2\theta$  XRD pattern of a 750Å film. Note the high intensity and the sharpness of the peaks. The inset depicts the  $\phi$ -scan of the {103} family peaks with a four-fold symmetry, showing the good epitaxy of the film.

Fig2: Evolution of the in-plane [202] (i.e.  $100_C$ ), and the out-of-plane parameter [040] (i.e.  $001_C$ ) of PCMO films with different thickness. The inset depicts the evolution the ratio between the in-plane and the out-of-plane parameters. Full lines are only a guide for the eyes.

Fig3:  $\rho(T)$  under different magnetic field (0, 5T and 9T) applied in the plane of the substrate for different films (a): 150Å, (b): 750Å and (c): 1100Å. Arrows indicate the direction of the temperature variation.

Fig4: Resistivity vs magnetic field at 75K, 100 K and 125K for a 1100Å film. Runs in field-increasing and field-decreasing are denoted by arrows. Note the large hysteretic region.

Fig5: In-plane magnetization vs magnetic field at 70K, 100 K and 120K for a 1100Å film. Runs in field-increasing and field-decreasing are denoted by arrows. The inset shows the magnetization vs temperature recorded under a magnetic field of 1.45T. The magnetization of the substrate was measured at each temperature and field and subtracted point by point.

Fig6: Electronic phase diagram of a 1100Å PCMO thin film determined by the critical fields.  $H_c^+$  and  $H_c^-$  are respectively taken as the inflexion points in  $\rho(H)$  in for up and down sweeps. In the dashed region, both CO insulating and metallic state are coexisting.

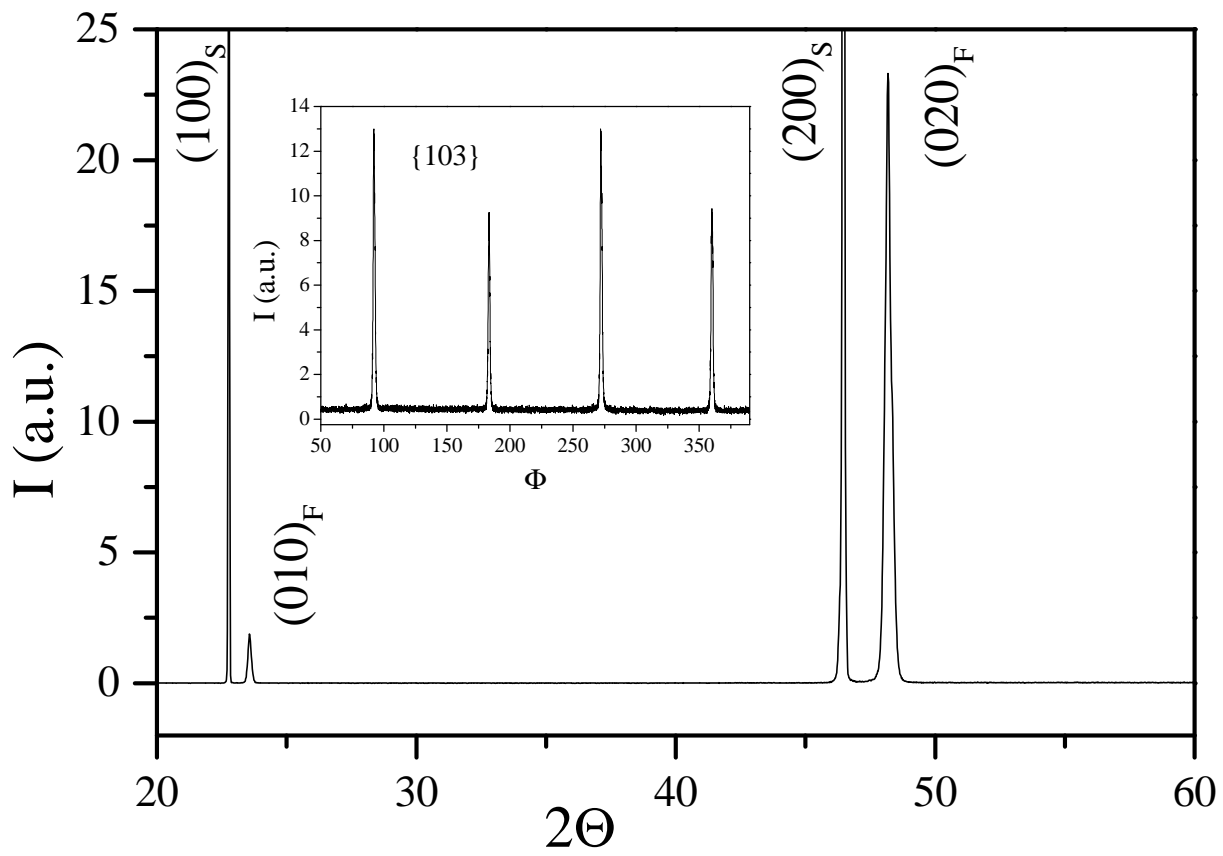


Fig. 1

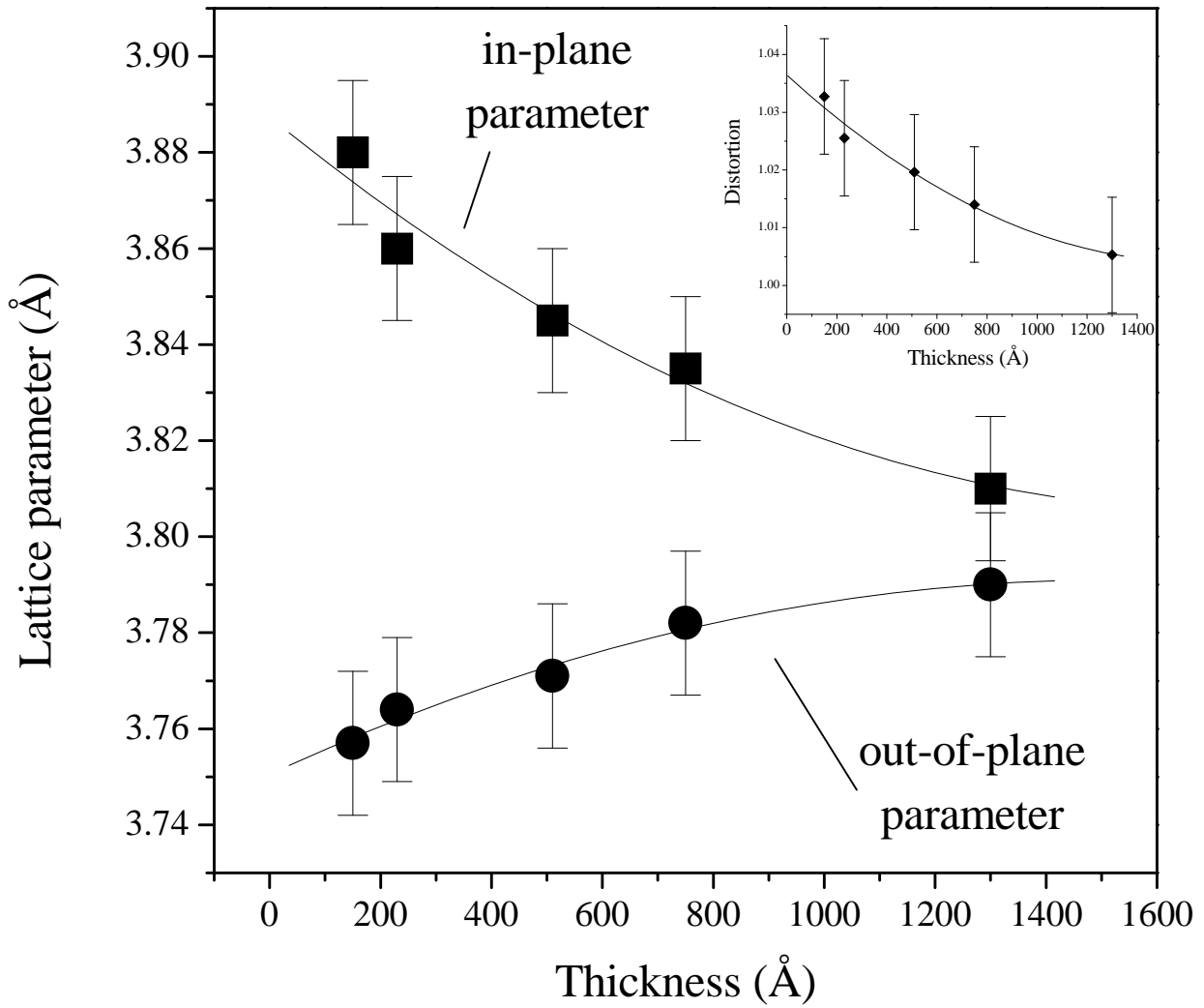


Fig.2

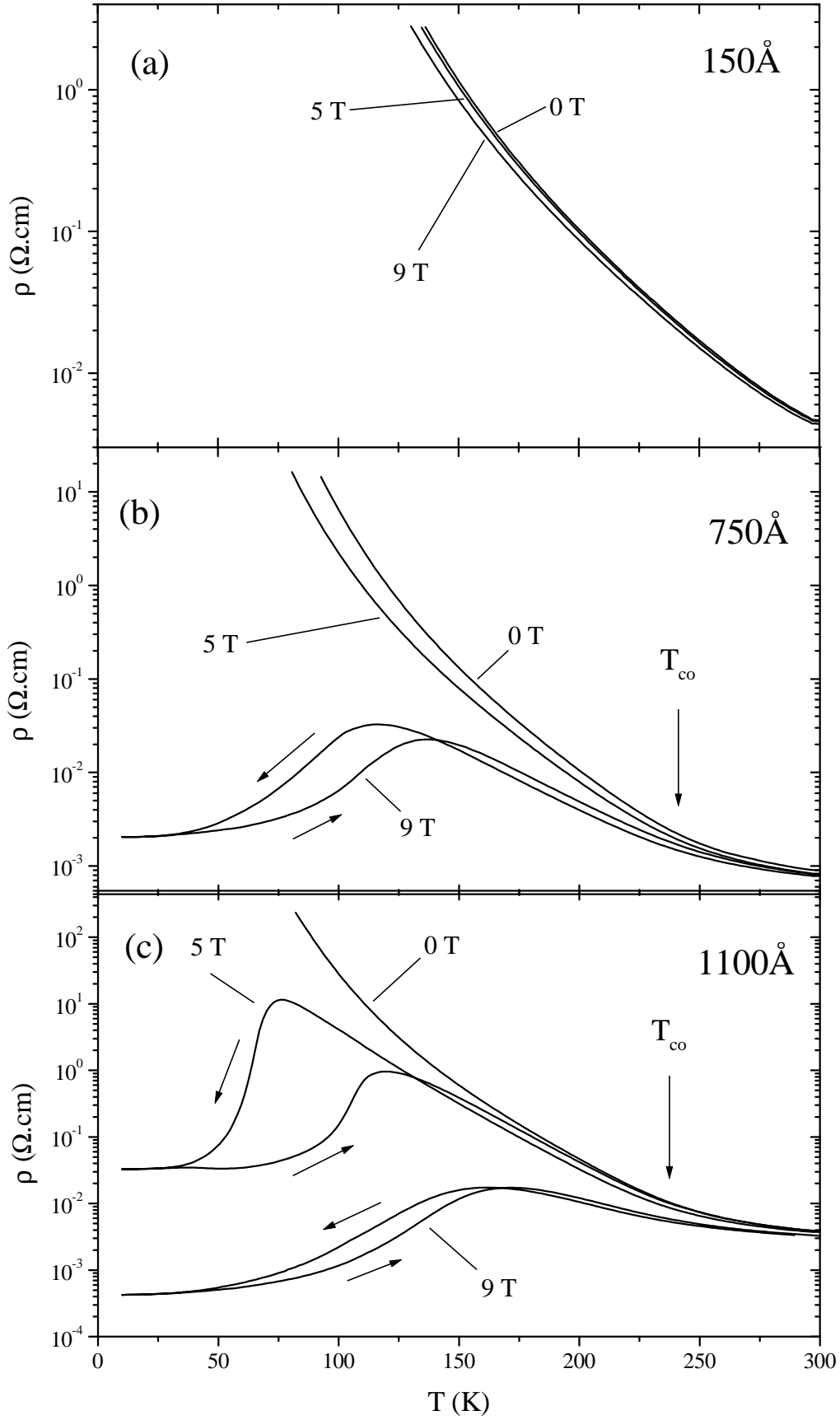


Fig.3

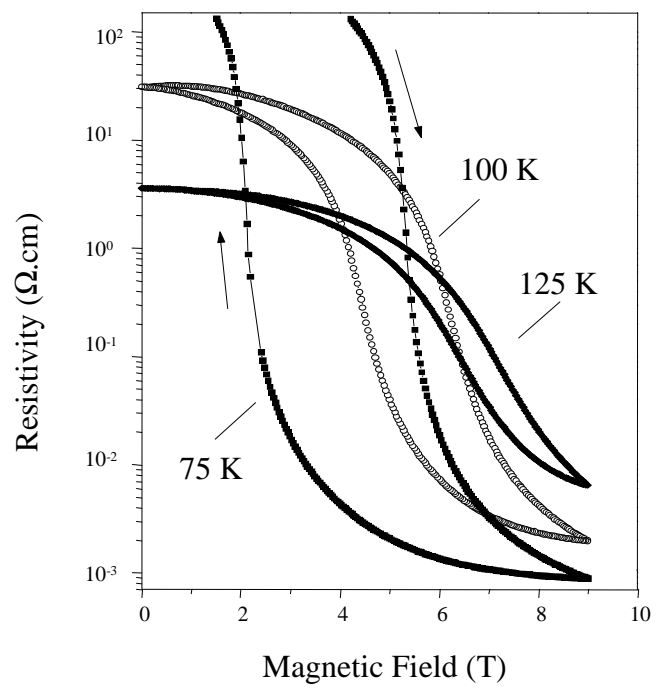


Fig.4

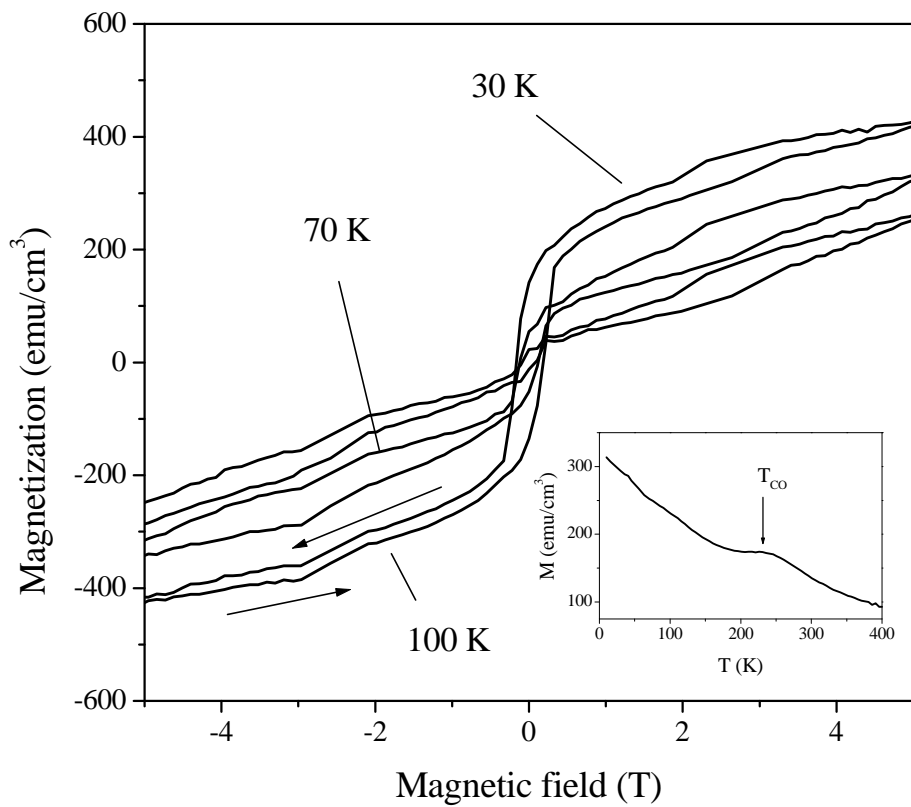


Fig.5

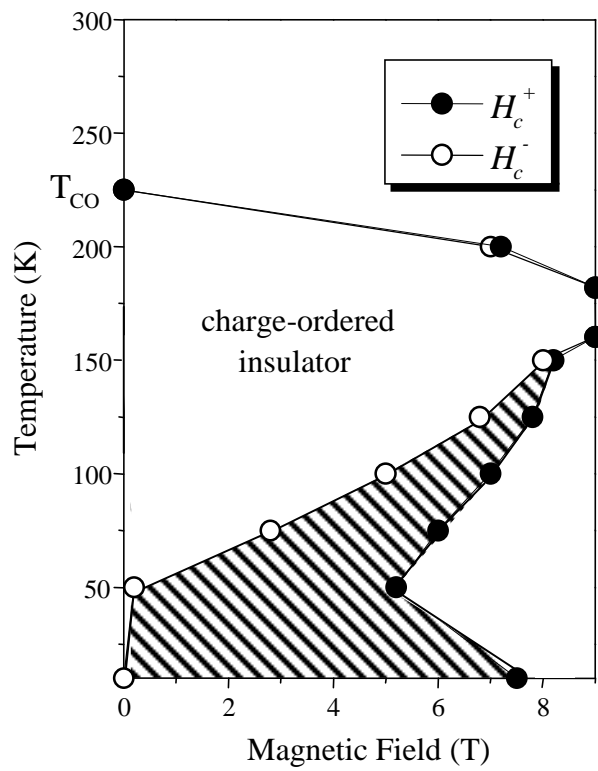


Fig.6